Breakout from the hot CNO cycle via the ^{18}Ne$(\alpha,p)^{21}$Na reaction

W. Bradfield-Smith, T. Davinson, A. DiPietro, A. M. Laird, A. N. Ostrowski, A. C. Shotter, and P. J. Woods
Department of Physics and Astronomy, University of Edinburgh, Edinburgh EH9 3JZ, United Kingdom

S. Cherubini, W. Galster, J. S. Graulich, P. Leleux, L. Michel, A. Ninane, and J. Vervier
Institute de Physique Nucléaire, UCL, Louvain-la-Neuve, Belgium

J. Görres and M. Wiescher
University of Notre Dame, Notre Dame, Indiana 46556

J. Rahighi
Van de Graaff Laboratory, Tehran, Iran

J. Hinnefeld
Indiana University, South Bend, Indiana 46634
(Received 19 January 1999)

The reaction ^{18}Ne$(\alpha,p)^{21}$Na, of importance to nuclear astrophysics, has been studied directly using the postaccelerated radioactive ^{18}Ne beam available at Louvain-la-Neuve and a gaseous helium target. This study covered the energy region from 2.04 to 3.01 MeV in the center of mass, and identified various levels in the compound nucleus ^{22}Mg. The stellar reaction rate due to these states has been deduced. The experimental rate shows good agreement with theoretical predictions [J. Görres, M. Wiescher, and F. K. Thielemann, Phys. Rev. C **51**, 392 (1995)] above 2.5 GK. [S0556-2813(99)02906-4]

PACS number(s): 97.10.Cv, 25.60.Je, 26.50.+x, 27.30.+t

I. MOTIVATION

Explosive hydrogen burning is thought to be the main source of energy generation in novae and x-ray bursters, and also provides an important route for nucleosynthesis of material up to masses as high as the mass 100 region via the rp process [1]. Up to a temperature of $T\sim0.2$ GK the burning with carbon takes place through the series of reactions,

$$^{12}\mathrm{C}(p,\gamma)^{13}\mathrm{N}(p,\gamma)^{14}\mathrm{O}(\beta^+)^{14}\mathrm{N}(p,\gamma)^{15}\mathrm{O}(\beta^+)^{15}\mathrm{N}(p,\alpha)^{12}\mathrm{C}$$

known as the hot CNO cycle. At higher temperatures, $T\sim0.4$ GK, the ^{14}O waiting point is bypassed by the series of reactions

$$^{14}\mathrm{O}(\alpha,p)^{17}\mathrm{F}(p,\gamma)^{18}\mathrm{Ne}(\beta^+)^{18}\mathrm{F}(p,\alpha)^{15}\mathrm{O}$$

with an increase in energy production. At still higher temperatures break-out from the cycle becomes possible.

The main reaction which determines the leak rate is ^{15}O$(\alpha,\gamma)^{19}$Ne [2]. However, in higher temperature situations it may be that other reactions provide alternative leak-out routes. In particular the reactions ^{18}Ne$(\alpha,p)^{21}$Na and ^{18}Ne$(2p,\gamma)^{20}$Mg have been suggested as possible candidates, although for the $2p$ reaction abnormally high densities would be required [3].

Any ^{19}Ne or ^{21}Na formed by these reactions acts as a seed for the rp process, where a series of charged particle reactions and β decays give mass flow to higher mass values. Thus the role of each possible breakout mechanism during such an event is vital in understanding the nucleosynthesis that would take place.

For the reaction ^{18}Ne$(\alpha,p)^{21}$Na no experimental information is available on the reaction strength. Indeed there is limited information concerning even the position of states in the compound system ^{22}Mg at and above the α particle threshold energy of 8.14 MeV. Estimates of the stellar reaction rate have been published by Görres and Wiescher [3]. As only two states in ^{22}Mg were known, at $E_x=8.29$ MeV and $E_x=8.55$ MeV, the rate was estimated from the level properties of the mirror nucleus ^{22}Ne [4] and from results obtained on the reaction ^{20}Ne$(^3\mathrm{He},n)^{22}$Mg [5]. A Hauser-Feshbach calculation using the code SMOKER was also used to help predict the stellar reaction rate. It is difficult to determine the uncertainty of these calculations since they are very sensitive to the parameters of isolated resonances; therefore for such reactions direct measurements, if possible, are very important.

The Radioactive Ion Beam (RIB) facility at Louvain-la-Neuve has developed a post accelerated ^{18}Ne beam. We report here some first results of a direct measurement of the reaction ^{18}Ne$(\alpha,p)^{21}$Na, in inverse kinematics, using the ^{18}Ne beam in conjunction with a gaseous helium target.

II. EXPERIMENTAL TECHNIQUE

The ^{18}Ne beam in the 3^+ charge state and with an energy of 30 MeV had a typical intensity of 5×10^5 pps during this experiment. Data was collected over a four day period.

Details of the detectors, the scattering chamber and the analysis method developed for investigating (α,p) reactions with a radioactive beam and extended gas target are presented in Ref. [6], which describes the investigation of the ^{13}N$(\alpha,p)^{16}$O reaction, which was used to test the feasibility

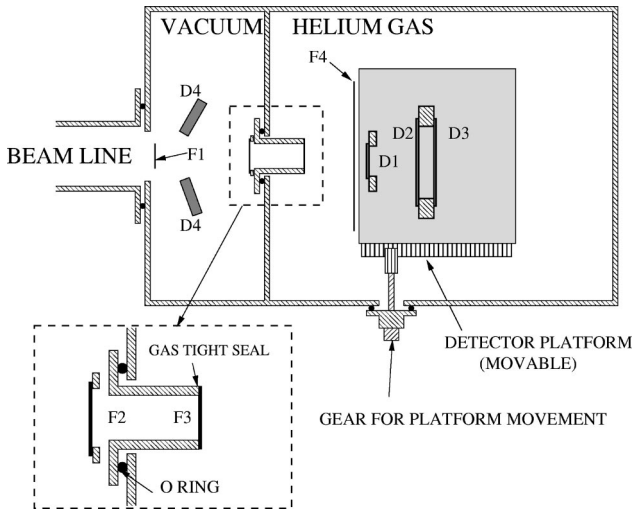

FIG. 1. A schematic view of the scattering chamber and detectors used. The detectors D1, D2, and D3 are double sided silicon strip detectors of thicknesses 63 μm, 300 μm, and 500 μm, respectively, and allow the reconstruction of trajectory for protons. The detectors D4 are surface barrier detectors used for the normalization of the beam current. The foil F1 was a thin carbon foil for beam diagnostics, F2 a gold foil of thickness 200 μg/cm^2 used for normalization of the beam current, F3 a nickel window of thickness 2 mg/cm^2 with a gold flash of 35 μg/cm^2 to contain the helium gas target, and F4 a nickel foil of thickness 5.8 mg/cm^2 to stop beam particles from damaging the silicon detectors.

of this method. The ^{13}N$(\alpha,p)^{16}$O reaction was chosen as the cross section was calculable from previous work on the inverse reaction ^{16}O$(p,\alpha)^{13}$N [7–9]. This ^{13}N$(\alpha,p)^{16}$O investigation showed that an $\omega\gamma$ value could be extracted with an accuracy of about 30% using this technique.

For the present investigation, the experimental method described in Ref. [6] was modified to allow a larger energy scan in the center of mass system, c.m., of ^{18}Ne$+\alpha$. This was done by using a thick nickel entrance window of 2 mg/cm^2 (Fig. 1) and a beam energy of 30 MeV. The beam energy in the laboratory, the LAB energy, upon entering the gas target was $\sim$16.3 MeV. With the 2 mg nickel window the helium gas target was contained at a pressure of 500 mbar, giving an energy loss through the gas of $\sim$1.3 MeV/cm. Data was collected with the detector system at two positions, giving an energy scan in the c.m. of 2.04–3.01 MeV for the first position, and an energy scan of 2.32–3.01 MeV for the second position.

III. RESULTS

A. Experimental data

The protons were identified using a ΔE-E technique with the energy from the front detector, D1, supplying the ΔE and the energy from the rear detectors, D2 and D3, supplying the E. The ΔE-E spectrum is shown in Fig. 2. It was known from the previous experiment that background protons would be seen due to the elastic scattering of protons from water vapor on the surfaces of all foils. Therefore, equal time was spent running with the gas target chamber under vacuum and filled with the helium gas, so as to properly understand the background and to allow background removal.

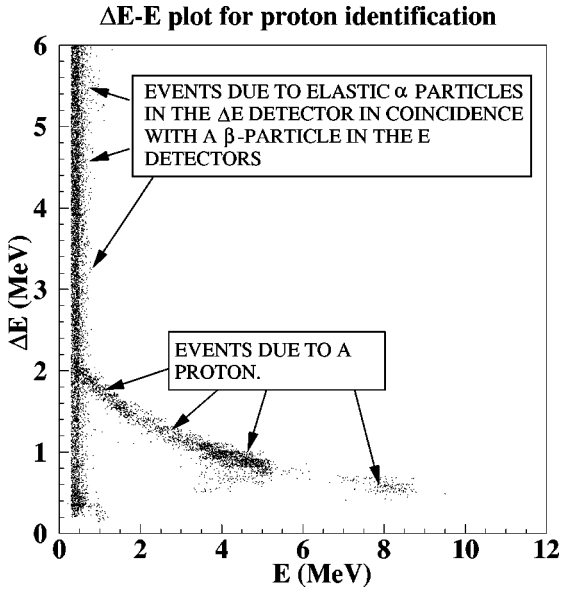

FIG. 2. The ΔE-E energy spectrum, with detector D1 as the ΔE and detectors D2 and D3 as the E, was used to gate on proton events for further analysis.

The detector system allowed the trajectory and energy to be reconstructed for each proton event as explained in Ref. [6]. The proton energy spectrum obtained with the target volume filled with helium gas and an energy scan from 2.04–3.01 MeV, along with the background spectrum obtained with no gas in the target volume is shown in Fig. 3.

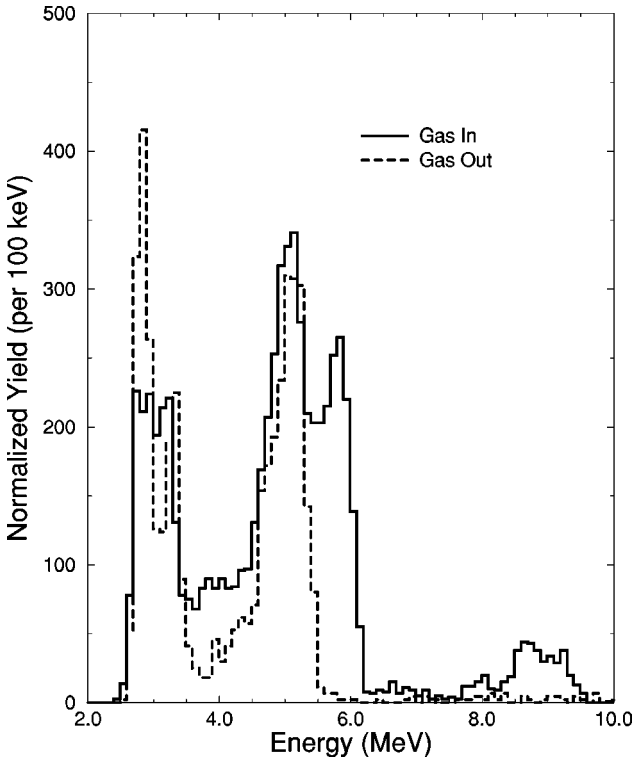

FIG. 3. Proton energy spectra for the target volume filled with helium gas, gas in, and for the target volume evacuated, gas out. The protons seen with no gas target are mainly due to the elastic scattering of protons from H_2O molecules on the surfaces of foils F2, F3, and F4.

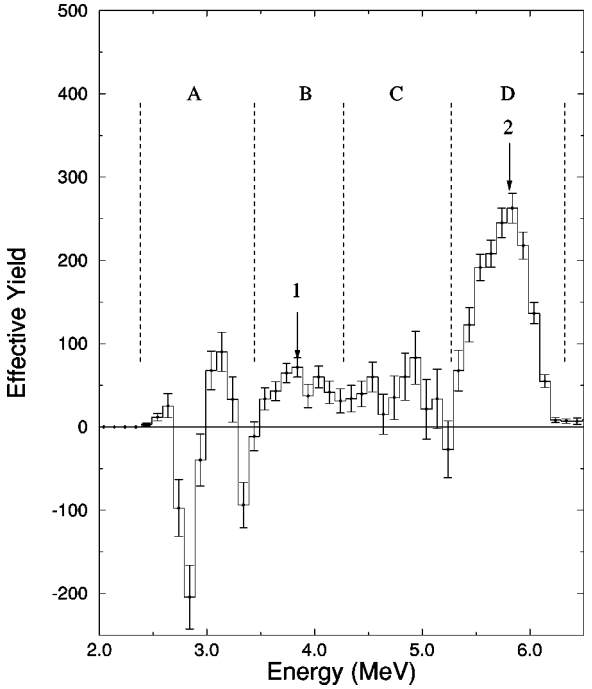

FIG. 4. Proton energy spectrum after background removal from 2–6 MeV. The energy regions of interest are marked by letters and peaks identified with confidence above the background are numbered.

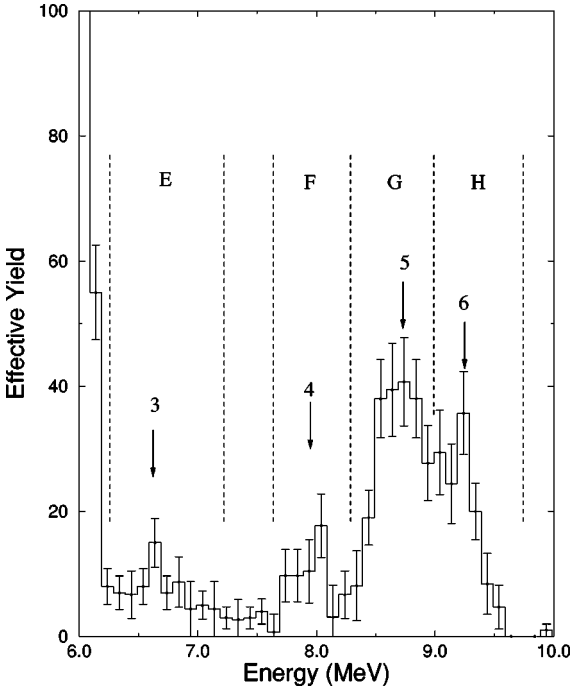

FIG. 5. Proton energy spectrum after background removal from 6–10 MeV. The energy regions of interest are marked by letters and peaks identified with confidence above the background are numbered.

The background spectrum, with gas out, has been normalized to allow direct comparison with the spectrum obtained with gas in [6]. These energy spectra are for proton events that have had their energies corrected for energy losses in the nickel foil (F4 in Fig. 1), in the dead layers on detector surfaces and in the gas. The proton energy spectrum after background removal is shown in two parts, in Figs. 4 and 5, which show at least six proton groups above the background in the energy regions marked B,D,E,F,G and H, these proton groups are labeled 1–6. Energy region A shows large fluctuations due to the background removal itself; the proton background in this energy region is significantly altered by the removal of the gas target, allowing no comparison to be made between gas in and gas out in this region. As the target thickness for the contaminants responsible for the background is not known, and may well change with time, no conclusions may be reached on the presence of the small peak seen in energy region C, which is strongly influenced by the background peak. A yield for each of the six proton groups was extracted, after the subtraction of the background had taken place.

The resolution of the proton groups seen in these spectra is roughly 400 keV. This width is due mainly to the large angular range covered by the proton telescope (0–33 degrees) and the width of the resonance. If the reaction mechanism is known, i.e., the level fed in the residual nucleus ^{21}Na, then it is possible to correct these proton peaks for the angular spread, as will be shown later. The straggling of proton energy due to energy losses is $\sim$50 keV and is negligible compared to these effects.

Each proton group was selected for further analysis using an energy window. The c.m. energy in the $^{18}\mathrm{Ne}+\alpha$ was then reconstructed assuming that reactions could take place to the ground state and the first six known excited states [10] (at energies of 0.332 MeV, 1.716 MeV, 2.425 MeV, 2.798 MeV, 2.829 MeV and 3.544 MeV) of the residual nucleus ^{21}Na. For a possible level assignment in the residual nucleus to be made for a proton group, the resulting reconstructed c.m. energy must lie within the energy range scanned experimentally, that is 2.04–3.01 MeV. Due to the experimental geometry such a level assignment is not necessarily unique and more than one possibility may exist. All reconstructed beam energy spectra seen hereafter were corrected for the change in efficiency through the extended gas target, to give a renormalized yield over 100 keV bins. This efficiency function was calculated using Monte Carlo techniques [6].

For proton group 1 there were four possible level assignments that could be made; these are to the levels at 2.425, 2.798, 2.829 and 3.544 MeV in the residual nucleus ^{21}Na (see Fig. 6). It can be seen that the energy resolution is better than indicated in the proton spectrum, since a kinematic correction for angle has effectively been made in Fig. 6. It is interesting to note that the 3.544 MeV state of the residual nucleus ^{21}Na decays by proton emission to the ground state of ^{20}Ne with a branching ratio of $\sim$100% [10]. This decay proton has an energy of $\sim$1.0 MeV in the c.m. of ^{21}Na which would correspond to an energy of $\sim$3 MeV in the LAB frame. If the reaction $^{18}\mathrm{Ne}(\alpha,p)^{21}\mathrm{Na}$ were indeed feeding the 3.544 MeV level then we would expect to observe a coincidence between the proton from the reaction and the subsequent decay proton. In Fig. 7 we show a 2D proton energy spectrum for two proton coincidence events. In this spectrum, we can see a small number of coincidence events in the correct energy region, possibly due to protons originating from the reaction $^{18}\mathrm{Ne}(\alpha,p)^{21}\mathrm{Na}$ leading to the 3.544 MeV state with an energy of $\sim$4 MeV, in coincidence with

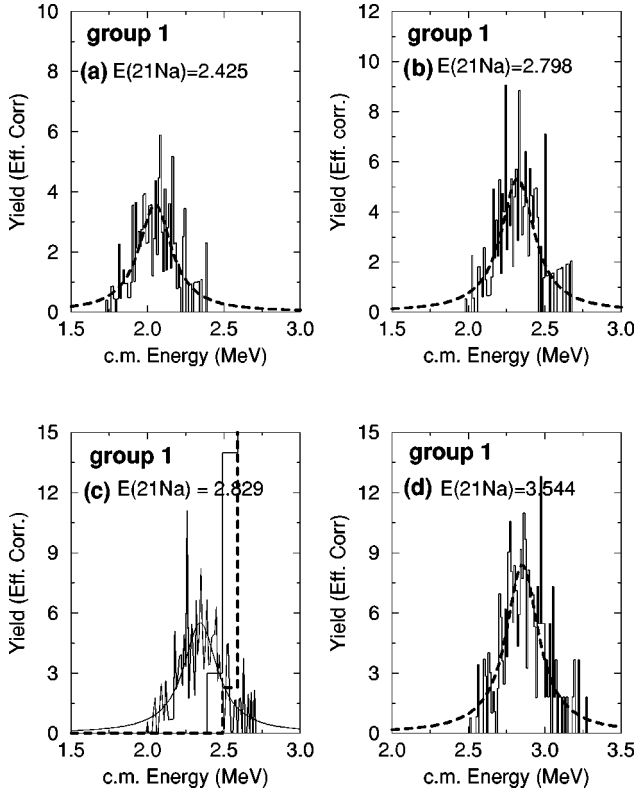

FIG. 6. Reconstructed c.m. beam energy spectra for proton group 1 assuming transitions to excited states of ^{21}Na at 2.425 MeV (a), 2.798 MeV (b), 2.829 MeV (c), and 3.544 MeV (d). The dashed lines are Lorentzian fits to the data.

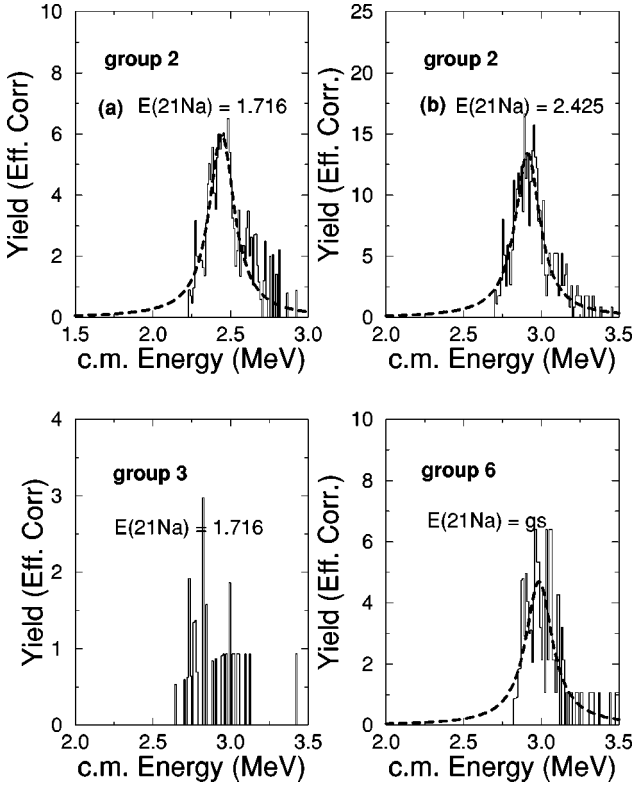

FIG. 8. Reconstructed c.m. beam energy spectra for proton group 2 assuming transitions to excited states of ^{21}Na at 1.716 MeV (a) and 2.425 MeV (b). Proton group 3 is reconstructed assuming that the 1.716 MeV level is accessed and proton group 6 assuming a ground state transition. The dashed lines are Lorentzian fits to the data.

protons with an energy of $\sim$3 MeV originating from the subsequent decay of the residual nucleus ^{21}Na. A Monte Carlo simulation of the reaction to the 3.544 MeV level, followed by the subsequent proton decay, gives a value for the fraction of 2 proton coincidence events to single events

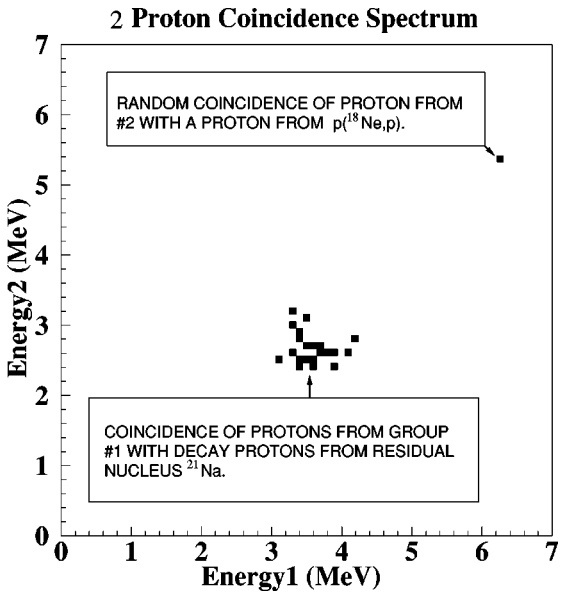

FIG. 7. Two proton coincidence spectrum. All points plotted correspond to two proton events, selected using ΔE-E information. For every two proton coincidence event the highest proton energy is plotted as energy1 in this figure.

of 0.075 ± 0.01. The experimental fraction is 0.09 ± 0.02. Within these errors, it is then possible to conclude that the most likely level assignment for proton group 1 is to the 3.544 MeV state. This Monte Carlo simulation also showed that the decay protons would not give a yield in the gated region B, and in fact these events lie in region A, which is dominated by the background proton events. For an estimate of the random coincidence rate for two protons from the reaction ^{18}Ne$(\alpha,p)^{21}$Na for the more intense proton peak (seen in Fig. 3 at an energy of $\sim$6 MeV), a rough calculation shows that we would expect to see 1 random coincidence event every 10 days. We in fact observe one event in this energy region over two days so this event is consistent with a random coincidence (Fig. 7).

For proton group 2 there are two possibilities [shown in Figs. 8(a) and 8(b)]. For groups 3 and 6 only one level assignment was possible (also shown in Fig. 8). For proton groups 4 and 5 there were two possible levels that could be accessed in the residual nucleus (see Fig. 9). A Lorentzian fit to each of these beam energy spectra of Figs. 6, 8 and 9 allows the resonance parameters to be found for each possible assignment (see Table I).

B. Resonance levels and strengths

In the cases where only one possible level assignment may be made, definite information may be deduced on the energy of the corresponding level in ^{22}Mg. From the beam energy spectra for proton groups 1 and 6 we can identify

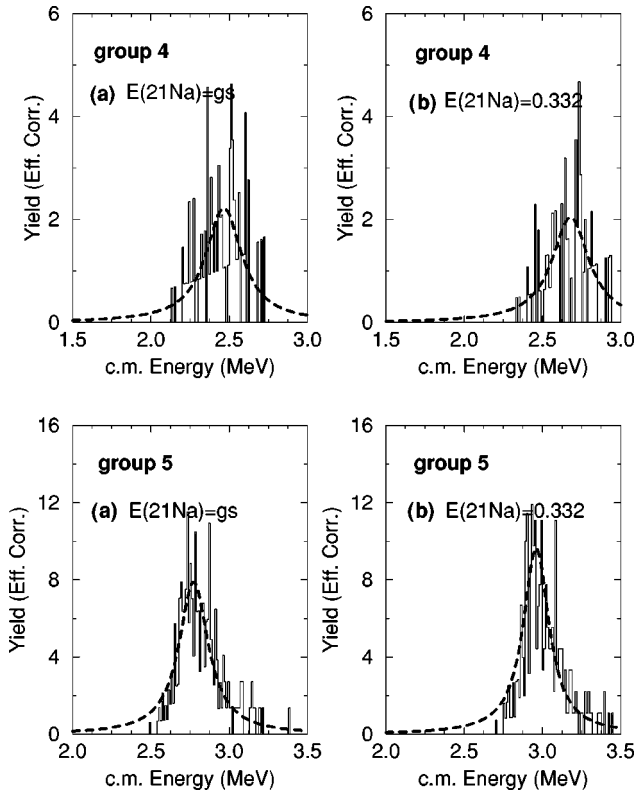

FIG. 9. For proton groups 4 and 5 there are two possible level assignments. The graphs marked 4(a) and 5(a) show the beam energy spectra for groups 4 and 5 for a transition to the ground state of the residual nucleus, and the graphs marked 4(b) and 5(b) show the beam energy spectra of proton groups 4 and 5 for a transition to the first excited state of ^{21}Na at 332 keV.

with certainty the presence of two levels in the compound nucleus ^{22} Mg, at 10.99 MeV and 11.13 MeV, respectively.

When, however, there are two possible level assignments, as for groups 2, 4 and 5, then no definite statement about the level structure of ^{22}Mg may be made. For group 2 the transition could be through levels of ^{22}Mg at 10.58 or at 11.05 MeV. For group 4 through levels at 10.6, corresponding to the 10.58 MeV level already identified, or 10.82 MeV. For group 5 through levels at 10.91 or 11.13 MeV, corresponding to the 11.13 MeV level observed from proton group 6. No conclusions may be reached based upon proton group 3 due to the low statistics and large errors in the fit to obtain the resonance parameters. The possible level structure in the compound system, due to all possible level assignments, is shown in Table II.

TABLE I. Resonance parameters extracted from the beam energy spectra seen in Figs. 6, 8, and 9.

Proton group	Level assignment in ^{21}Na (MeV)	E_R (MeV)	Γ (keV)
1	3.544	2.85 ± 0.05	310 ± 63
2	1.716	2.44 ± 0.05	195 ± 18
	2.425	2.913 ± 0.05	195 ± 18
3	1.716	2.8 ± 1.0	
4	g.s.	2.46 ± 0.06	300 ± 100
	0.332	2.68 ± 0.06	300 ± 100
5	g.s.	2.77 ± 0.05	218 ± 30
	0.332	2.96 ± 0.05	218 ± 30
6	g.s.	2.99 ± 0.06	210 ± 50

TABLE II. $\omega\gamma$'s for the various possible assignments. The level that would be accessed, for each assignment, in the compound nucleus is also shown.

Proton group	Level assignment in ^{21}Na (MeV)	$\omega\gamma$ (keV)	State in ^{22}Mg (MeV)
1	3.544	$2.8^{+3.0}_{-1.7}$	10.99
2	1.716	$7.1^{+3.0}_{-2.5}$	10.58
	2.425	$26^{+30.0}_{-10.0}$	11.05
3			
4	g.s.	$0.77^{+.35}_{-0.3}$	10.6
	0.332	$1.0^{+0.7}_{-0.5}$	10.82
5	g.s.	$3.82^{+3.9}_{-1.5}$	10.91
	0.332	$8.7^{+9.2}_{-5.0}$	11.13
6	g.s.	$4.24^{+4.0}_{-2.5}$	11.13

The low statistics and the limited angular range are such that no reliable fits can be made to the data to extract the angular momentum in the exit channel from the proton angular distribution. Thus nothing definite may be said about spins of the observed states. However, as an $l=0$ transition is more likely than an $l=2$ transition due to the increased height of the barrier, an $l=0$ transition has been assumed for all the proton groups seen experimentally. With this assumption, it is possible to evaluate the most likely spins of the natural parity states accessed in the compound nucleus though it must be stated that these spins are very tentative.

The c.m. proton energy spectrum, recalculated assuming that proton group 2 feeds the 2.425 MeV state, proton group 4 feeds the ground state and that proton group 5 feeds the 0.332 MeV state, and corrected for kinematic broadening, may be seen in Fig. 10. The level scheme for ^{22}Mg in the region investigated by this work may be seen in Fig. 11. The solid lines indicated in the level scheme for ^{22}Mg are for those levels identified with some confidence, while the dashed lines indicate possible levels only. This figure also shows the the decay of the 3.544 MeV excited state of the residual nucleus ^{21}Na proton emission.

The extraction of resonance strengths from the data requires knowledge of the resonance parameters, which were obtained from the fits seen in Figs. 6, 8 and 9 and the efficiency of the solid state detector system as a function of c.m. energy and position within the extended gas target $\varepsilon(E,x)$. The efficiency, $\varepsilon(E,x)$, was determined using a Monte Carlo calculation which assumed an isotropic distribution in the c.m. system. The resonance strengths are then calculated using the equation [6]

$$\omega\gamma=\frac{2\mu x_0 Y}{\pi N_t N_b \Gamma\hbar^2}\left(\int_0^{x_0}\int_0^{\infty}\frac{\mathrm{Prob}(E,x)\varepsilon(E,x)}{E((E-E_r)^2+\Gamma^2/4)}dEdx\right)^{-1}, \quad (1)$$

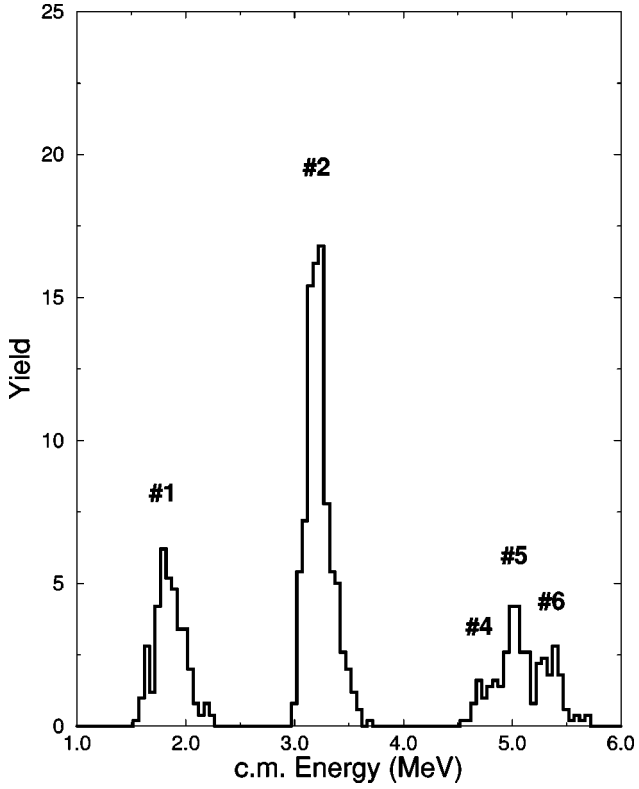

FIG. 10. The recalculated c.m. energy spectrum for proton groups 1, 2, 4, 5 and 6. Events in the regions dominated by elastic events, marked A and C in Fig. 5, are not selected for reconstruction, which includes those protons produced by the decay from the 3.544 state in ^{21}Na, accessed by proton group1.

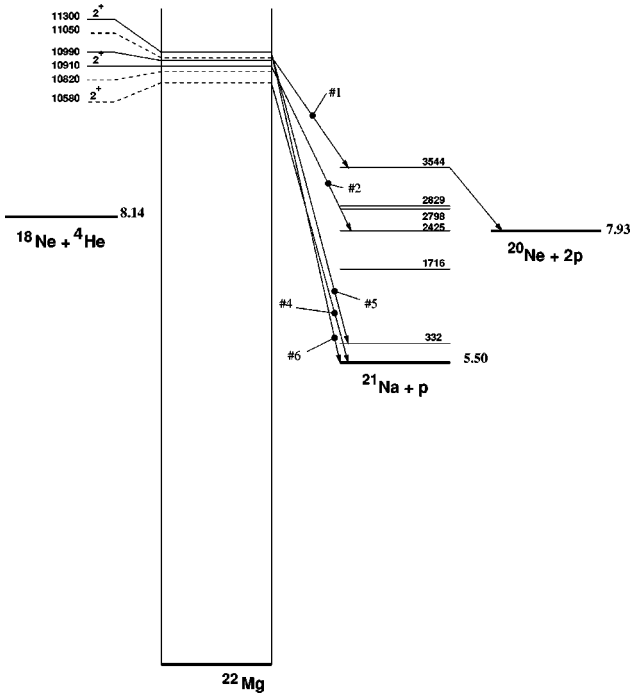

FIG. 11. Level scheme diagram for the reaction ^{18}Ne$(\alpha,p)^{21}$Na. Spins are only given for those levels were a definite spin can be calculated, assuming an isotropic transition in the c.m. and thus an $l=0$ final state.

where μ is the reduced mass of the entrance channel, x_0 is the length of the extended gas target, Y is the yield, N_t is the gas target thickness, N_b is the integrated beam current and Prob(E,x) is the probability of the beam having an energy E at a position x in the extended gas target. The $\omega\gamma$'s obtained for each of the proton groups with errors are detailed in Table II.

The main source of error in the values for $\omega\gamma$ is due to the uncertainty in the mean beam energy as the beam enters the gas target. As the resonance energy increases in magnitude, the distance from the window to the point of highest proton yield decreases. Thus the error in the mean beam energy at entrance causes the largest error for the resonance at the highest energy, nearest the entrance window. For those proton groups believed to be at the highest energy seen, 11.13 MeV in ^{22}Mg, the error bars are of order 100%. These errors are higher than the 30% expected [6] due to the increased thickness of the window used to contain the gas and the increased error in the beam energy upon entrance into the gas volume.

The same proton groups were observed for both positions at which the detector system was situated. The change in efficiency for data gathered at the two positions allows us to compare values for the resonance strengths, $\omega\gamma$'s, calculated at the two positions. For proton group 2 the $\omega\gamma$ resulting from the assumption that the reaction, ^{18}Ne$(\alpha,p)^{21}$Na, feeds the 1.716 MeV state of the daughter nucleus, ^{21}Na, results in a value of 17.82 ± 2.0 PkeV, whilst the assumption that the 2.2425 MeV state is fed results in a value for the resonance strength of 39.0^{+40}_{-15}. Comparing these values for the resonance strength of proton group2 with those listed in Table II shows agreement between the values obtained with the assumption that the 2.425 MeV state is fed in the daughter nucleus ^{21}Na. For proton groups 4 and 5 the uncertainty in level assignment is not resolved by considering this additional piece of information.

C. Stellar reaction rate

The stellar reaction rate is given by

$$\langle\sigma v\rangle=\left(\frac{8}{\mu\pi}\right)^{1/2}\frac{1}{(kT)^{3/2}}\frac{\pi\Gamma\omega\gamma\hbar^2}{2\mu}\times\int_{E_R-\Gamma}^{E_R+\Gamma}\frac{\exp\left(-\frac{E}{kT}\right)}{[(E-E_R)^2+\Gamma^2/4]}dE, \quad (2)$$

where μ is the reduced mass, T is the temperature, and k is Boltzmann's constant. A narrow resonance is not assumed as the width, Γ is greater than kT and thus the Boltzmann distribution changes significantly over the resonance. The integration is performed over the region to which the Breit-Wigner cross section is a good fit to the experimental data. The resulting stellar reaction rate per mol for each proton group may be seen in Fig. 12. Errors in $\omega\gamma$, E_R, and Γ are taken into account for the evaluation of the total error in the stellar reaction rate by performing the calculation with the limiting values of the various parameters, however, the error bounds are not shown in this figure, but are shown in Fig. 14. This calculation assumes that proton group 2 is accessing the

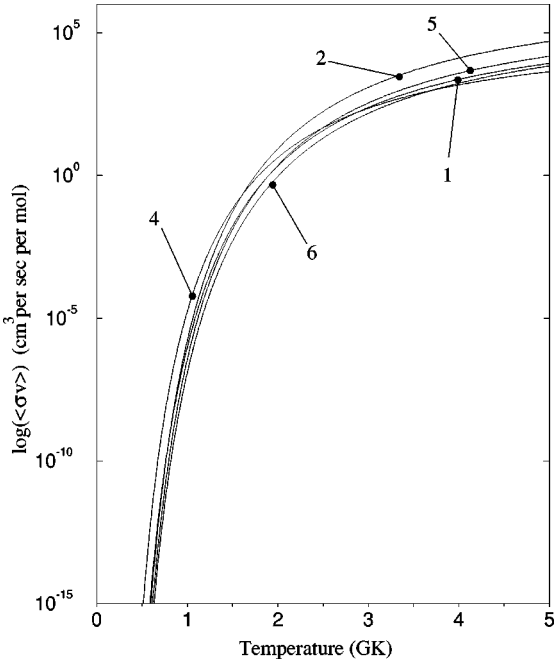

FIG. 12. The stellar reaction rates per mol calculated for each of the five proton groups of importance for the reaction ^{18}Ne(α,p)^{21}Na. No errors are shown in this plot.

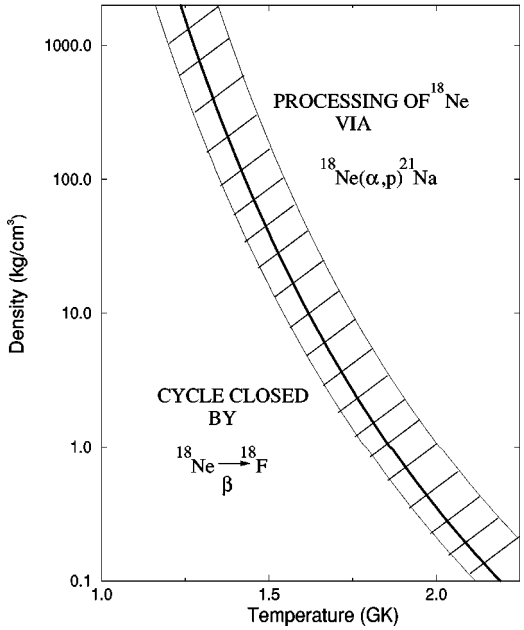

FIG. 13. The onset of burning via ^{18}Ne(α,p)^{21}Na.

2.425 MeV state of ^{21}Na, proton group 4 is accessing the ground state of ^{21}Na and that proton group 5 is accessing the 0.332 MeV state of ^{21}Na. In this figure the stellar reaction rate is dominated by proton group 2 at temperatures above 1.8 GK and by proton group 4 below 1.8 GK.

The mean lifetime of ^{18}Ne in a stellar environment due to destruction by helium nuclei depends only upon the density and the temperature, and is given by the expression [11]

$$\tau_m(\mathrm{He}) = \frac{1}{N_{\mathrm{He}}\langle \sigma v \rangle}, \tag{3}$$

where N_{He} is the number of helium nuclei per cm^3, calculated assuming a helium mass fraction of 0.25. As this destruction via reaction competes with destruction via β^+ decay we have two regimes. One in which any ^{18}Ne formed β decays to ^{18}F and one in which the reaction ^{18}Ne(α,p)^{21}Na allows mass flow out of the hot CNO cycle. This is illustrated in Fig. 13. The thick line is a locus for which the mean life time due to destruction via the reaction ^{18}Ne(α,p)^{21}Na and the mean life time due to decay are equal. The thin lines are the upper and lower limits for this calculation. It should be noted that this locus is calculated for the observed states only. The discovery of further states can only act to reduce the lifetime with respect to reaction for all temperature and density conditions.

IV. DISCUSSION

The total stellar reaction rate may be seen in Fig. 14, calculated using the assumed level assignments stated above. The upper and lower limits are taken from limiting values of level parameters and $\omega\gamma$'s and the different level assignments possible. A comparison of the stellar reaction rate calculated from this work with the theoretical predictions made by Görres and Wiescher [3] shows reasonable agreement above 2.5 GK. For temperatures below 2.5 GK however, the stellar reaction rate falls far below the predicted values. This is due to the fact that the calculation of stellar reaction rate from this work has been made using only the observed resonances between 2.4 and 3.0 MeV (c.m. of ^{18}Ne+α), whereas the theoretical calculation used predicted resonance strengths at lower energies from an energy of 0.15–2.00 MeV in the c.m. system. Thus the agreement above 2.5 GK indicates that the observed resonances dominate the reaction rate in this region. At lower temperatures the reaction rate

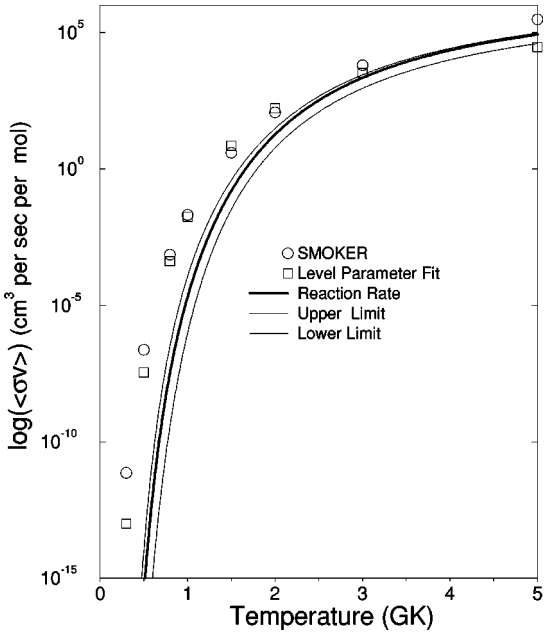

FIG. 14. The total stellar reaction rate per mol for the ^{18}Ne(α,p)^{21}Na reaction is given by the thick line. The two thin lines give the upper and lower limits calculated using the limiting values. The SMOKER rate and the level paramter fit shown are detailed in Ref. [3].

will be dominated by states in the compound nucleus ^{22}Mg with lower energy and with weaker resonance strengths. Further work will need to be done in order to investigate this reaction at lower energies to check the theoretical prediction in the temperature region below 2.5 GK.

The consideration of lower energy resonances in the calculation of lifetime can only cause the lifetime to decrease for any temperature and density conditions. It is therefore interesting to note that for a temperature of 1.5 GK and a density of 1000 kg/cm^3, typical conditions for the surface layer of an x-ray burster, that any ^{18}Ne present in a stellar gas will be destroyed via the reaction $^{18}\mathrm{Ne}(\alpha,p)^{21}\mathrm{Na}$.

Resonances at a lower energy will have a smaller yield due to the effect of the Coulomb barrier and so any successful measurement in the future will depend crucially upon the elimination of the proton background seen in Fig. 6. A more precise geometry is also required to remove the uncertainty in the beam energy responsible for observed proton events. The increased beam intensity of ^{18}Ne beams that may be available at Louvain-la-Neuve or at new Radioactive Beam facilities will also help bring experimental measurements into a wider region of astrophysical interest.

ACKNOWLEDGMENTS

We would like to thank the technicians and workshop at the RIB facility in Louvain-la-Neuve for their valuable contribution to this work, especially Paul Demaret and Roger Versin. This work has been partly financed by the Interuniversity Poles of Attraction Program-Belgian State, Prime Minister's Office-Federal Office of Scientific, Technical and Cultural Affairs and NATO grant GRG.940213. We would also like to thank UK EPSRC (Engineering and Physical Sciences Research Council) for their support for this work.

[1] A.E. Champagne and M. Wiescher, Annu. Rev. Nucl. Part. Sci. **42**, 39 (1992).
[2] K. Langanke, M. Wiescher, and F.K. Thielemann, J. Astrophys. Astron. **301**, 629 (1986).
[3] J. Görres, M. Wiescher, and F.K. Thielemann, Phys. Rev. C **51**, 392 (1995).
[4] E.R. Flynn, Ole Hansen, and O. Nathan, Nucl. Phys. **A228**, 189 (1974).
[5] W. Alford *et al.*, Nucl. Phys. **A457**, 317 (1986).
[6] W. Bradfield-Smith *et al.*, Nucl. Instrum. Methods, Phys. Res. A (to be published).
[7] S.E. Woosley, J. Astrophys. Astron. **186**, 601 (1973).
[8] W. Gruhle and B. Kober, Nucl. Phys. **A286**, 523 (1977).
[9] A.V. Nero and A.J. Howard, Nucl. Phys. **A210**, 60 (1973).
[10] R.B. Firestone, *Table of Isotopes* (Wiley, New York, 1996).
[11] C.E. Rolfs and W.S. Rodney, *Cauldrons in the Cosmos* (University of Chicago Press, Chicago, 1988).